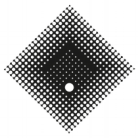

Firebrand transport from a novel firebrand generator: numerical simulation of laboratory experiments

Firebrand transport from a novel firebrand generator: Numerical simulation of laboratory experiments

Running head: Experimental and numerical study of firebrand

R. Wadhwani[A,B,] , D. Sutherland[B,C], A. Ooi[B,D], K. Moinuddin[A,B,*]

[A]Centre for Environmental Safety and Risk Engineering, Victoria University, Melbourne, VIC 3030, Australia

[B]Bushfire and Natural Hazards CRC, Melbourne, VIC 3002, Australia

[C]School of Science, University of New South Wales, Canberra, ACT 2600, Australia

[D]Department of Mechanical Engineering, University of Melbourne, VIC 3052, Australia

Abstract

Firebrands (often called embers) increase the propagation rate of wildfires and often cause the ignition and destruction of houses. Predicting the motion of firebrands and the ignition of new fires is therefore of significant interest to fire authorities. Numerical models have the potential to accurately predict firebrand transport. The present study focuses on conducting a set of benchmark experiments using a novel firebrand generator, a device that produces controlled and repeatable sets of firebrands, and validating a numerical model for firebrand transport against this set of experiments. The validation is conducted for the transport of non-burning and burning cubiform firebrand particle at two flow speeds. Four generic drag sub-models used to estimate drag coefficients which are suited for a wide variety of firebrand shapes are verified

* Corresponding author: khalid.moinuddin@vu.edu.au

for their applicability to firebrand transport modelling. Among four, these sub-models are found to be good in various degrees at predicting the transport of firebrand particles.

Keyword: Short-range firebrands, Lagrangian particles, Firebrand generator, Fire Dynamics Simulator, Drag models; Lateral spread; Contour; Contour peak location;

Summary

A combined experimental and numerical study of firebrand transport is presented. A novel firebrand generator is built to produce specific-shaped burning firebrands and measure landing distributions. A physics-based model is used with four different drag sub-models to reproduce experimental results and results are obtained with various degrees of fidelity.

Introduction

Firebrands are a primary cause of increased rate of fire spread inside a forest canopy and can cause damage to structures located close to a forest. The whole process encompassing the transport of the firebrands and the propensity to ignite surface fuels or structures is called spotting. Short-range (where the firebrands travel up to 750 m) spotting is principally observed inside the forest canopy where the firebrands travel mainly due to shear stress of wind, with little to no lofting provided by the buoyant force of the sub-canopy fire (Cruz *et al.* 2015). Massive short-range spotting can increase the observed rate of fire spread up to three times, compared with the rate of fire spread when the firebrands are not present; this effect is observed in the 1962 Daylesford fire (McArthur 1967). Thus, it is imperative to account for short-range spotting in the fire spread simulations explicitly, especially for vegetation types such as eucalyptus and pine forests, which produce significant numbers of firebrands. It is extremely challenging to conduct field-scale measurements due to safety hazards to personnel and equipment during the experiment, as well as the associated expenses and the limits of

experimental parameters that are achievable. To the best of the authors' knowledge, there are some field-scale research studies with actual vegetation (Gould *et al.* 2008; El Houssami *et al.* 2016; Filkov *et al.* 2017; Thomas *et al.* 2017; Storey *et al.* 2020) which have quantified the short-range spotting distances, firebrand material, sizes, and mass, from a forest with limited parameters affecting the firebrand transport.

Numerical approaches to quantify the behaviour of short-range spotting offer more convenience to develop a short-range firebrand model that can be incorporated in the operational fire model. Tarifa and his co-workers (Tarifa *et al.* 1965; Tarifa 1967) were the first who attempted to develop a correlation between different types of firebrand and their maximum spotting distance. However, their work focused on firebrands, which were lofted by the plume representing long-range spotting firebrands, to develop a spotting model. Similarly, Albini (Albini 1979) also developed a spotting model for long-range firebrands which has been widely used in various operational fire models. Stephen & Fernandez-Pello (Stephen and Fernandez-Pello 1998) carried out numerical modelling for spherical metallic firebrand particles (representing sparks from power cable) and wooden firebrand particles coming from a tree. The work focused on understanding the firebrand trajectory ejected at a certain height from the ground in the surface layer flow (30-50 m from ground) and their ignition potential to cause spotting. However, they did not develop any correlation which could be used in an operational fire model representing various type of firebrands in a wildfire. Sardoy *et al.* (Sardoy *et al.* 2008) conducted the first numerical study where a correlation between short-range firebrand with the fire size. Sardoy *et al.* simulated firebrand transport by conducting a three-dimensional (3D) physics-based modelling for the transport of different disc-shaped firebrand from the plume generated in a line fire source. They developed a correlation between firebrand parameters and ambient parameters like fire intensity and wind speed. Their model revealed a bimodal distribution of

67 the firebrands on the ground downstream when both pyrolysis and char oxidation are present
68 in the firebrand. Some of the firebrands, mostly in a flaming state, land at a short-distance from
69 the source fire and other firebrands in charring state land at a long-distance from the source fire.
70 However, the quantification of error and uncertainty associated with their model is not
71 computed nor is the model compared with any field scale experiments or real wildfire incidents.

72 Simulations results from physics-based fire models must be carefully validated against
73 experiments with burning firebrands. The validation of a model is challenging at field scale
74 because of difficulties in controlling experimental parameters which affect the repeatability of
75 the experiment. These challenges can be exacerbated by the settlement of communities close to
76 forests, which restricts the location of the experiment. An alternative is to conduct the validation
77 work at laboratory scale and then scale up the simulations and compare with documented
78 wildfire incidents (Linteris *et al.* 2004).

79 The firebrand dragon constructed by National Institute of Standards and Technology (NIST),
80 USA (Manzello *et al.* 2008) is one such apparatus which can produce artificial firebrand
81 showers in a meticulous and repeatable manner. The NIST firebrand dragon has been mainly
82 used to study the impact of firebrands on structures (Manzello and Suzuki 2013, 2014; Suzuki
83 *et al.* 2016) and ignition of forest surface fuel (Manzello *et al.* 2006). Kortas *et al.* (Kortas *et*
84 *al.* 2009) validated a particle transport model for the transport of cylindrical and disc-shaped
85 firebrands used in the NIST firebrand dragon. They compared mass loss and longitudinal travel
86 distance distribution, although, they ignored the collisions between the firebrand particles with
87 the wall of firebrand dragon. The NIST firebrand dragon has a bend at the mouth which
88 produces a Dean's vortex near the mouth (Wadhwani *et al.* 2017b). The Lagrangian assumption
89 for particle modelling would not be valid to use in the validation with the NIST firebrand dragon
90 due particle interactions and modification of flow due to large number of particles. It is to be

91 noted that Kortas *et al.* (Kortas *et al.* 2009) assumed a Weibull distribution of firebrands leaving
92 the dragon mouth as initial condition to match with the experiments. Wadhwani *et al.*
93 (Wadhwani *et al.* 2017b) constructed a firebrand generator prototype which produces a uniform
94 shower of firebrands to validate the Lagrangian particle model of Fire Dynamics Simulator
95 (FDS). FDS is a physics-based fire model which has been extensively used in fire science for
96 building and wildland fire (McGrattan *et al.* 2015a). However, their work was limited to testing
97 the performance of inbuilt drag model of FDS for non-burning particles.

98 The present work is built upon Wadhwani *et al.* (Wadhwani *et al.* 2017b) to study burning
99 firebrands by constructing an entirely new firebrand generator. Compared to Wadhwani *et al.*
100 (Wadhwani *et al.* 2017b) there are two main improvements in the generator. The generator
101 descried here is constructed of stainless-steel material to produce uniform burning firebrands
102 which was not possible in the prototype generator constructed of PVC. The new generator also
103 allows control of the flow Reynolds numbers, accommodates different sizes of firebrand, and
104 can produce a wide range of combusting firebrands. The experimental data itself is valuable as
105 a benchmark set for any model validation. Realistic firebrands are found to be considerably
106 different in size, shape and stages of combustion as observed in field studies (Gould *et al.* 2008;
107 El Houssami *et al.* 2016; Filkov *et al.* 2017; Thomas *et al.* 2017; Storey *et al.* 2020). While
108 there has been some work on cylindrical firebrands (Tohidi and Kaye, 2017) firebrand particles
109 are often assumed purely spherical (Thomas *et al.* 2020, Thurston *et al.* 2017). This assumption
110 will likely lead to significant inaccuracies in predicted landing distributions. A simplifing
111 assumption for long-range firebrands is a constant terminal velocity, which has been shown to
112 over-predict the landing density of firebrands (Thomas *et al.* 2020). Therefore, accounting for
113 the shape of the firebrand is critical towards improved predictions of firebrand distribution. It

114 is also necessary to quantify differences between predicted and actual firebrand distribution to
115 assess upper and lower limits of error.

116 Thus, the purpose of the computational study is twofold: (a) quantify the assessment for a set
117 of alternative drag models suited to represent generic shape of firebrands using the firebrand
118 generator and (b) validating the firebrand transport model within a physics-based model (FDS)
119 for burning firebrands. The validated model can then be applied to study the transport of short-
120 range firebrands such as firebrand transport inside a forest canopy (Wadhwani *et al.* 2019).

121 **Experimental methodology and design of firebrand generator**

122 The base design of the firebrand generator is based on the prototype detailed in Wadhwani *et*
123 *al.* (Wadhwani *et al.* 2017b). The critical modifications on the base design are (i) addition of a
124 firebrand heater to ignite firebrands (Fig. 1(a-c)) and (ii) insertion of a honey-comb-type flow
125 straightener (Fig. 1(d)) to minimise the length required to develop a uniform flow at the mouth
126 of the generator. The combined length of two concentric stainless-steel pipes is 3.9 m which
127 consists of two pipes of nominal inner diameters 50 and 200 mm and of lengths 2.3 and 3.1 m,
128 respectively. The generator is constructed to produce varied size and shapes of firebrand with
129 different degrees of combustion and at different flow speeds, however, for the current study,
130 only burning and non-burning cubiform firebrand particles and two Reynolds numbers of the
131 flow are studied as a proof of concept.

132 >> Figure 1 here >>

133 Fig. 1 shows the different sections of the concentric pipe firebrand generator (known as the
134 Victoria University Stainless Steel Generator or VUSSG). Fig. 1(a) and (b) shows the front and
135 back view of the firebrand generator highlighting the main component of the equipment. Fig.
136 1(e) provides a cutaway schematic of the firebrand generator clarifying the working principles

137 of our firebrand generator. Air is drawn into the equipment through the 'air inlet' (shown in
138 Fig. 1(a)) by using a centrifugal fan (hidden inside the cabinet denoted as 'Fan'). The air then
139 reaches the annular region of the concentric pipes (shown in Fig. 1(e)) and passes through a
140 honeycomb flow straightener. The flow provides the required acceleration to the firebrand
141 particles coming through the inner pipe. The 3-phase induction motor centrifugal fan of 7.457
142 kW runs at 2860 rpm in the hidden cabinet that provides air to the firebrand generator. The
143 motor controller is used to control the speed of a fan, and thus, provides a control on flow
144 Reynolds number. The firebrands are fed to the 'firebrand heater' (sketched in Fig. 1(f)) which
145 conveys firebrands providing them sufficient time to ignite and maintain a flaming combustion
146 state (Fig. 1(c)) before they falls into the 'firebrand inlet' pipe via a 'chute' (Fig. 1(a), (e)). The
147 'firebrand heater' consists of a conveyor belt and two (top and bottom) radiant heating elements
148 that are designed to give firebrand feed rates 0.055-0.165 firebrands.sec^{-1}. By adjusting the
149 conveyor belt speed it is possible to achieve 40% to 75% combusted cubiform firebrand
150 particles when both heating elements are turned on. The low firebrand feed rate is to ensure
151 there is effectively only one-way coupling between the fluid and the particle; an essential
152 feature of Lagrangian model. That is, while the fluid exerts forces upon the particle, the particle
153 has a negligible effect on the flow. In a particle-laden flow the presence of many particles can
154 induce turbulence and particle-particle interactions can occur (Lain and Garcia 2006). These
155 phenomena are not included in the Lagragnian particle model. In a real, ember laden flow, we
156 expect the ember density to be sufficiently low that a Lagranian model is sufficient (Thomas *et*
157 *al.* 2020, Thurston *et al.* 2017). A higher ember feed rate is possible but is beyond the current
158 scope of research. The average initial mass of pine radiata based cubiform firebrand particles,
159 which are used in this study, is 0.83 g and the average length is 12.45 mm identical to the
160 particles used by Wadhwani *et al.* (Wadhwani *et al.* 2017b). During non-burning firebrand
161 experiments the heating elements and pilot flame are turned off. During the burning firebrand

experiments the conveyer belt runs at 0.165 firebrands/second corresponding to 40% combusted cubiform firebrand. The firebrand heater provides a net radiative heat flux (measured using handheld radiometer) of 25 $kW.m^{-2}$ with the firebrands fed to the conveyor belt of the firebrand heater at an ambient temperature of 30°C. Inside the firebrand heater, a firebrand particle heats for 45 (±2) s, exposed to net radiative heat flux of 25 $kW.m^{-2}$ and then convert into flaming combustion for 24 (±2) s through auto-ignition or piloted ignition by a small flame while continuously receiving radiant heat flux before the firebrand falls into the chute to the firebrand inlet location.

The firebrand temperature after the firebrand leaves the heater but before it is injected into the inner pipe at the 'firebrand inlet' location (Fig. 1(a), (e)) of the generator is measured manually and quickly using a non-contact infrared thermometer and thermocouple to cross-verify the experimental measurement. 30 firebrands (i.e. 12% of firebrands used in each experimental run) were paused between the heater and inlet and measured using a noncontact infrared thermometer (with emissivity 0.97) and using a manual contact thermocouple. The measured average temperature with the infrared thermometer was 300°C and the thermocouple was 320°C, so the average temperature of the firebrand particle is taken as 310 (±50) °C. The average mass of firebrand particle before injected at 'firebrand inlet' is reduced by 57.4%; the average volume is reduced by 27.1%, and average density is reduced by 20.7% respectively to its initial ambient measurement. The effective heat of combustion of the firebrand particle is 16.21 $MJ.kg^{-1}$, the heat of reaction is 522.39 $kJ.kg^{-1}$, and soot yield is 0.00192 $kg.kg^{-1}$ (the measurement techniques for these quantities are detailed in Wadhwani (2019).

The firebrand generator is utilised to generate a series of firebrands (after flow has been established to a steady-state condition) which lands on the 'distribution grid' (20×20 cm) (Fig. 1(b)); the firebrand may then bounce and land again. Only the first-impact locations where the

firebrand initially lands are measured using two high-speed cameras. The video footage is post-processed using MATLAB to extract the firebrand-impact location (Wadhwani, 2019). The video footage is firstly processed to exaggerate contrast between the particle, the marked grid lines in the landing area, and the white background. The franes were then displayed and manually inspected to record the impact location. In each experimental run 250 firebrands are used and collected, and the experimental runs are conducted until the convergence criteria (Eq. 1 and 2) are met. Experiments were run at least eight times to satisfy the criteria and the resulting cumulative distribution overall experimental runs are considered the experimental distribution of cubiform firebrands.

$$P_i(x,y) = \frac{1}{i}\sum_{j=1}^{i} \frac{f_j(x,y)}{\int_{y_l}^{y_u}\int_{x_l}^{x_u} f_j(x,y)dxdy} \quad , \qquad (1)$$

where i is the number of experiments, $f_j(x,y)$ is the distribution of particles for an experiment j. x_l, y_l, x_u, y_u are the lower and upper coordinates of the distribution grid x, y. Equation (1) takes the observed distributions from experiment j, normalises the distribution so the integral is one (and thus the summand is a probability density function) before averaging the distribution over i experiments.The distribution is deemed converged (Eq. 2) when the successive variation in each distribution grid is found to be less than 5%. This level of statistical convergence is found to be sufficient, a higher convergence criteria could be considered but would significantly increase the number of experimental runs (including data processing) required to achieve a high convergence level at each grid point. The convergence criteria is defined as,

$$max\{P_{i+1}(x,y) - P_i(x,y)\} < 0.05 \; . \qquad (2)$$

The Lagrangian particle model validation required the measurement of the flow velocity and particle velocity. The flow velocity is measured with a Pitot tube. The particle velocity is

208 measured using two using two orthogonal high-speed cameras. The measurement methodology
209 and uncertainty associated with the measurements are discussed in Wadhwani *et al*. (Wadhwani
210 *et al.* 2017b). The experiments are carried out at the higher-end of the flow Reynolds numbers
211 observed in real wildfire during short-range spotting (Gould *et al.* 2008; Thomas *et al.* 2017),
212 two flow speeds, representative of fire conditions, are considered in this study denoted as the
213 Re-1 case (Re no. 3×10^5) and Re-2 case (Re no. 3.4×10^5). The video footage of particle tracking
214 at the mouth is post-processed in MATLAB to measure the distance a particle travels between
215 individual image frames to compute particle component velocities. The average values of
216 particle velocity for all cases are listed in Table 1. Note that u is the streamwise velocity along
217 the axis of the tube, w is the vertical velocity of the particle which is positive in the upwards
218 direction measured from the centre of the tube, v is the spanwise velocity of the particle
219 mutually orthogonal to u and w; the positive direction follows from the standard right-hand
220 rule. The v- and w-particle velocities arise because of the irregular insertion of particles,
221 turbulence in the tube of the generator, rotation of the particles themselves, and collisions with
222 the walls of the generator.

223 >> Table 1 here >>

224 **Numerical Model**

225 The numerical model that we seek to validate is Fire Dynamics Simulator (FDS) (ver. 6.2.0).
226 FDS solves the basic governing conservation equations for mass, energy, and momentum of a
227 Newtonian fluid at low-Mach number using a second-order finite difference method. The
228 details of the equations and solution method are provided in the technical guide (McGrattan *et*
229 *al.* 2015b) and hence are not discussed here. FDS uses the Large-Eddy Simulation (LES)

methodology with the Deardoff turbulence model to describe the gas-phase turbulence and a Lagrangian particle model to describe the solid particle transport.

FDS has an inbuilt drag model only for spherical and cylindrical shapes (McGrattan *et al.* 2015b), for cubiform particles whose initial, unburnt, sphericity is 0.806, it can be assumed that the spherical drag model would be sufficient. Sphericity (Wadell, 1933) is the surface area of a sphere with equal volume of the particle, divided by the surface area of the particle. As the particle combusts the sphericity will change, however, over a short combustion time the sphericity is unlikely to change significantly enough to effect the drag coefficient in some meaningful way. The effect of sphericity and tumbling of particle will tend to average out on the distribution grid of 20 cm wide which was already observed for non-burning cubiform firebrands (Wadhwani *et al.* 2017b). This aspect is a crucial assumption for short-range spotting, such as occurs inside a forest canopy, where particles have short-flight time as compared to long-range spotting and the focus of the present study. Moreover, it is important to explore replacing the existing drag model in FDS with a generic drag model that could be used to represent a generic shape of firebrand which is neither spherical nor cylindrical. Thus, four drag models found in the literature are selected which are widely used and applicable to a generic shape of particle-based on its sphericity, for this reason no direct comparisons of drag coefficient were attempted. These models are the Haider and Levenspiel (Haider and Levenspiel 1989), Ganser (Ganser 1993), Hölzer and Sommerfeld (Hölzer and Sommerfeld 2008), and Bagheri and Bonadonna (Bagheri and Bonadonna 2016) drag models; the details can be found in Table 2.

>> Table 2 here >>

Fig. 2 shows the representation of different drag models used in present study for cubiform particle with two vertical lines representing an approximate variation of Reynolds number during the flight time of firebrand particles. The Reynolds number used is based upon the particle length scales:

$$\mathrm{Re_p} = \frac{\rho_{\mathrm{air}}\, \mathrm{L}_{particle}}{\mu_{air}(T)} |\mathrm{V_{particle}} - \mathrm{V_{flow}}|) \tag{256}$$

Where the $v_{subscript}$ refers to the velocity of the particle or flow, ρ is the density, and μ the (temperature dependent) viscosity and L is the particle length (McGrattan et al. 2015b).

The variation occurred due to dissipation of flow velocity from the mouth to downstream. Near the ground the Reynolds number is approximately 3×10^3 and near the mouth of the generator, at the higher flow velocity, the Re is approximately 3.5×10^5. The difference between FDS inbuilt and drag models found in the literature is due to simplification of drag law adopted for spherical particles in FDS. Hölzer & Sommerfeld (Hölzer and Sommerfeld 2008) have measured the difference between experimental and predicted drag coefficient by different drag models for different shapes. They observed that for cuboidal and cylindrical shape particles using Haider and Levenspiel, Ganser and their own drag model shows mean relative deviation in estimating drag coefficient by 42.3%, 38.4% and 29% respectively. Furthermore, they observed the maximum to minimum relative deviation in estimating drag coefficience varies by three orders of magnitude. Thus, inherently, the drag models found in literature already have significant differences but have been accepted for major engineering applications.

>> Figure 2 here >>

The combustion of firebrands are represented using the inbuilt FDS single-step mixing controlled model considers a single fuel species that is composed primarily of C, H, O, and N

274 that reacts with oxygen in one mixing-controlled step to form H_2O, CO_2, soot, and CO. The
275 details of the combustion model can be found in FDS technical guide (McGrattan *et al.* 2015b).

276 **Results**

277 The experimental measurement of flow profile at the mouth of the generator is shown for two
278 orthogonal directions (Y-, Z- direction) to the flow (X- direction) in Fig. 3. Uniform flow
279 develops at the mouth of the generator for both flow cases in the orthogonal directions to the
280 flow with velocity at centre (V_{centre}) to be 23.4 $m.s^{-1}$ and 25.9 $m.s^{-1}$ respectively. After
281 developing a uniform flow field, firebrand particles are injected in the stream as non-burning
282 and burning. The extremely low feed rate ensures no particle-particle collision and few
283 collisions with the wall of the pipe (0-2% in each experiment run). The particle velocity
284 component measured using high-speed camera are detailed in Table 1. Experimental
285 observations of firebrand distribution are compared to simulations.

286 >> Figure 3 here >>

287 The simulation domain encompasses the experimental apparatus from the mouth of the
288 generator to the distribution grid, similar to the work with the prototype generator (Wadhwani
289 *et al.* 2017b). The simulated distribution grid has the same dimensions as the experimental
290 distribution grid. The simulation domain is 10.2 m long, 2.4 m wide, and 2 m high respectively
291 in X, Y, and Z- directions. The domain is sub-divided into four parts longitudinally, $0 \leq x \leq$
292 $0.5, 0.5 \leq x \leq 2.5, 2.5 \leq x \leq 4.5$, and $4.5 \leq x \leq 10.2$ m with uniform grid sizes ($\Delta x=\Delta y=\Delta z$)
293 20, 40, 40 and 40 mm respectively. The mouth of firebrand generator is placed at x=0. The
294 centre of the generator mouth is placed 1.1 m above the ground. The simulation inlet condition
295 was defined using the time-averaged mean flow profile measured at the firebrand generator
296 mouth. The results are shown to be independent of the choice of grid at flow Reynolds' number

297 of 4×10^5 and discussed in Wadhwani (2019). Fig. 4 shows the simulated mean distribution (as
298 contours) of the flow speed of the experimental setup for both cases at the centre of mouth. The
299 presence of a strong jet flow is visible 3.5 to 4 m from the mouth.

300 >> Figure 4 here >>

301 After the flow establishment, firebrand particles are injected in the simulation with a
302 distribution of initial particle velocities given in Table 1.

303 A 27 combination of firebrand particles injected in the domain to thoroughly represent
304 experimental condition with an initial component velocity equal to $u \pm \sigma_u$, $v \pm \sigma_v$, and $w \pm \sigma_w$
305 (representing mean and standard deviation of particle component velocity given in Table 1).
306 Following the same methodology as Wadhwani et al. 2017 for non-burning cubiform particles
307 using a prototype firebrand generator, six types of Lagrangian particles are injected to represent
308 the particle distribution density. The six types of Lagrangian particles are defined by $\mu \pm \sigma/4$,
309 $\mu \pm 3\sigma/4$, and $\mu \pm 3\sigma/2$; μ, σ are the mean density and standard deviation of particle densities
310 respectively of cubiform particles. In the experiments, particles do collide with the duct.
311 However, the simulation is initialised with particles at the mouth of the generator with some
312 specified velocities. Therefore, particle collisions with the duct are not explicitly computed, but
313 their cumulative effect is somewhat captured in the initial velocities of the particles.

314 Comparative contours between experimental and simulated firebrand distributions are plotted
315 in Fig. 5-8 for simulations using various drag models. The supplementary file provides further
316 insight in the distribution of particles. In Fig. 5-8, the solid lines are the experimental
317 distribution. The dotted lines denote the equivalent simulated distribution; the simulated
318 distribution meets the same convergence criteria as experimental distribution.

319 >> Figures 5-8 here >>

For non-burning cubiform firebrand in Fig. 5 and 6 the simulated results overlap quite well in both the Re1 and Re2 cases with all drag models. The difference between the locations of two peaks i.e. experimental and simulated (computed using Eq. 8), is found to be less than 5% for non-burning cubiform firebrand with following drag models:

- Re 1: FDS default, Haider and Levenspiel, Ganser and Bagheri and Bonadonna
- Re 2: FDS default, Haider and Levenspiel and Bagheri and Bonadonna

The quantitative difference found between the two peaks for each case is presented in their respective figures for all the drag models. The difference between the two peaks is computed as a ratio of relative difference between the two peak locations from the mouth of the firebrand generator to the location of experimental peak as represented in equation 8.

$$difference_{peak\ to\ peak} = \frac{peak_{expt} - peak_{sim}}{peak_{expt}}, \qquad (8)$$

For burning cubiform firebrands in Fig. 7 and 8, peak difference is less than 5% with following drag models:

- Re 1: Haider and Levenspiel and Ganser
- Re 2: Haider and Levenspiel, Ganser, Bagheri and Bonadonna and Hölzer and Sommerfeld

In all figures (5-8), Haider and Levenspiel is the only drag model which resulted in less than 5% difference in peak location for all four configurations.

In all the simulations (shown in Figs. 5-8), the lateral spread of simulated firebrand particle overlaps well with the experimental observation. The difference in lateral spread of firebrands is found to be small i.e. 0-0.1 m or 0-7% of experimental width on either side of the peak of

distribution using Haider & Levenspiel model in all the simulations. For other drag models (including the FDS default), inconsistent differences are observed in lateral spread with differences varying by 0-0.5 m or 0-35% of experimental width on either side of the peak of distribution. The lateral spread is caused in part by the initial v- and w- components of the particle velocity which could be due to turbulence inside the firebrand generator. The lateral spread is also likely exacerbated by the rotation of the particles which will result in imbalanced drag forces and exaggerated (compared to a point particle) lateral movement. van Wachem *et al.* (2015) and Carranza and Zhang (2017) also observed similar phenomenon when studying transport of non-spherical particles in a confined domain. The present work considers only the point particle assumption used in FDS, which considers only the drag force acting on the particle and limits the inclusion of other forces acting on the particle.

The maximum distance of firebrand travel is different for each simulation. Fig. 9 shows the comparison of the peak of the firebrand distribution and maximum distance of firebrand spotting for cubiform particles using different drag models. The whiskers in the plot represent the maximum and minimum possible spotting distances for all the cases. The comparison between the non-burning and burning cubiform firebrands for both Re cases, shows that combustion of the firebrands significantly reduced the peak locations of the experimental and simulated firebrand distributions. The changes occur because of the significant reduction in particle mass and the slight reduction in particle size due to burning which reduces the momentum of firebrand when released from the mouth of firebrand generator. However, a few of them are able to travel farthest from the mouth of firebrand generator as observed in experiments which may be due to collision with surface of pipe. The burning firebrand particles are simulated as burnable fuel and could lose mass. However, because of the short flight time (~1-2 s), the mass loss of the particles over the simulated trajectory is negligible. The vegetation

365 pyrolysis model of FDS has been extensively validated for litter fuels (Perez-Ramirez *et al.*
366 2017; Wadhwani *et al.* 2017a; Wadhwani 2019) and multiple other materials (Moinuddin *et al.*
367 2020) and so we believe the simulation should provide a good estimate of the in-flight mass
368 loss of the experimental particles. Because the simulated mass loss is negligible over the flight
369 time, we do not believe that mass loss has significant effect on the landing distribution in the
370 experiments.

371 The Haider and Levenspiel drag model arguably gives a better comparative prediction of peak
372 location of firebrand distribution and maximum spotting distance as compared to other drag
373 models for burning firebrands. The Ganser model appears to be second best, because its Re-2
374 non-burning prediction is not as good as the Haider and Levenspiel model. Although the default
375 drag model provides a reasonable prediction for the non-burning firebrands, its prediction for
376 burning cases are not as good. In Fig. 2, within the Re range for this study (marked two vertical
377 lines), drag coefficients from Haider and Levenspiel, Ganser and Bagheri and Bonadonna
378 models are very close to each other and overall these models give better results other two
379 models.

380 When comparing the lateral distribution of firebrands predicted by Haider and Levenspiel
381 model (Haider and Levenspiel 1989) and Ganser model (Ganser 1993), it can be seen that the
382 Haider and Levenspiel model shows a consistent overlaps with the experimental spread. This
383 aspect becomes profound when other shapes, such as cylindrical and square-disc shaped
384 firebrand particles, are considered, as observed by Wadhwani (2019) and Wadhwani *et al.*
385 (2021) for non-burning particles. A similar comparison can be drawn for the maximum and
386 minimum spotting distances by comparing the whiskers in Fig. 9.

387 >> Figure 9 here >>

In this case, all of the particle distributions are two-dimensional and there are no well-established statistical tests, without significant limitations, to rigorously compare bivariate distributions. A bivariate Kolmogorov Smirnov test has been described in the literature, however, there is no rigorous way to order bivariate data. A discussion of the limitations for tests for bivariate distributions may be found in: Quill et al. (2020). It may be possible to develop a bespoke test for our datasets, but this is beyond the scope of the present work.

Conclusion

The movement of firebrand particles in a wildfire can be simulated using a Lagrangian model because the particles are too small to significantly alter the driving and pyrogenic winds. We constructed a novel firebrand generator that produces uniform flow with series of non-burning and burning firebrands with varied firebrand shape and sizes, flow speeds, and combustion stages. The firebrand generator was used to conduct a benchmark experiment which is used to validate a Lagrangian sub-model of Fire Dynamics Simulator (FDS) for cubiform firebrands, both non-burning and burning, at two flow speeds.

The simulated results using FDS were found to closely represent the experimental observation for the distribution of first-impact location of firebrands. The uncertainties in the measurements and simulations are quantified throughout the manuscript. The experimental distributions are allowed to converge until a maximum 5% variation, the uncertainties in the simulated distributions are quantified by the minimum and maximum statistics provided in Fig. 9, mean deviations in estimates of drag coefficients are provided as appropriate, and the difference between the peaks of the experimental and simulated distributions are quantified. The simulation was found to practically predict the lateral spread of firebrands with negligible differences 0-0.1 m (i.e. 0-7% of experimental width) on either side of the peak of distribution

411 using Haider & Levenspiel drag model. This difference in lateral spread is significantly higher
412 and inconsistent with other drag models. However, the peak location of firebrand distribution
413 using Haider and Levenspiel drag model is found to be slightly under-predicted (<5%)
414 compared to experimental peak location of distribution. The under-prediction could be due to
415 inherent error in estimating drag coefficient by the drag model (Hölzer and Sommerfeld 2008).
416 The maximum spotting distances with the non-burning firebrands are found to have good
417 agreement with the experimental observations with an over-prediction by 8-12% to the
418 experimental values. For the burning firebrands it was found there was the simulated maximum
419 spotting distance of cubiform firebrands was underpredicted by 15-20% compared to the
420 experimental values. The most likely reason for this issue is simplified representation of the
421 experiments while conducting simulations. In the experiments, there is a possibility that there
422 were a greater number of firebrands heavier than the averaged firebrand. Only a fraction of the
423 firebrands (30 out 250) were used to estimate properties of the firebrands required for
424 simulation.

425 The Haider and Levenspiel drag model, as compared to other drag models considered, was
426 found to be better suited for firebrands to estimate the firebrand distribution and this could be
427 used as an alternative drag model to study transport of firebrands with FDS. The FDS inbuilt
428 drag models are restricted to only two shapes of firebrand particle i.e. spherical and cylindrical.
429 The Haider and Levenspiel drag model presents an alternative choice as a generic shape factor
430 based drag model. However, further study, similar to the one here, is required at different
431 firebrand characteristics (e.g. size, shape, combustion phase) and flow speeds to fully quantify
432 the error associated in estimating spotting distance. Our novel firebrand generator can be used
433 to conduct such validation studies of Lagrangian sub-model with different shape, rate of

combustion, and Reynolds number in future studies. Some preliminary comparisons of different shapes appears in Wadhwani *et al.* (2021).

The models tested in this study were developed empirically, by curve fitting to the results of free-fall (rather than a forced flow) tests. All the models attempt to account for irregularly shaped particles by incorporating some estimates of sphericity of the particles. The Haider and Levenspiel model uses only the classical definition of sphericity, whereas Gasner introduces shape-factors, Holzer and Sommerfeld use an additional measure of cross-wise sphericity, and Bagheri and Bonadonna use an elongation and equivalent diameter of the particle. Because these models are essentially complicated functions which fit the observed it is difficult to appraise the features of each model in a different context based on the landing distribution data that we measured. Our results imply that more the complicated estimates of shape are not necessarily appropriate for estimating drag coefficients in our flows.

Extending the modelling to complete fire conditions is challenging. After modelling transport for general firebrand shapes, the most important factor is modelling the combustion of the firebrands along the flight path. The rate of combustion along the flight path would be particularly difficult to estimate, and the atmospheric conditions, such as a possibly reduced level of oxygen, would likely influence the combustion rate.

Data Availability Statement (DAS)

The data used to generate the results in the paper will be made available upon reasonable request.

Acknowledgement

The authors would like to acknowledge the technical supports provided by Mr Lyndon Macindoe and Mr Philip Dunn during the experimental study. We also acknowledge computational support provided by the Spartan HPC team of the University of Melbourne.

Conflict of interest

There is no conflict of interest.

Declaration of funding

The financial support for this study was provided by Bushfire and Natural Hazards CRC, Australia.

References

Albini, FA (1979) Spot fire distance from burning trees. Intermountain Forest and Range Experiment Station General Technical Report, Missoula, MT.

Bagheri, G, Bonadonna, C (2016) On the drag of freely falling non-spherical particles. *Powder Technology* **301**, 526-544.

Cruz, MG, Gould, JS, Alexander, ME, Sullivan, AL, McCaw, WL, Mathews, S (2015) 'Guide to Rate of Fire Spread Models for Australian Vegetation.' (CSIRO Land and Water Flagship, Canberra, ACT and AFAC, Melbourne, VIC:

El Houssami, M, Mueller, E, Filkov, A, Thomas, JC, Skowronski, N, Gallagher, MR, Clark, K, Kremens, R, Simeoni, A (2016) Experimental procedures characterising firebrand generation in wildland fires. *Fire Technology* **52**, 731-751.

Filkov, A, Prohanov, S, Mueller, E, Kasymov, D, Martynov, P, El Houssami, M, Thomas, J, Skowronski, N, Butler, B, Gallagher, M (2017) Investigation of firebrand production during prescribed fires conducted in a pine forest. *Proceedings of the Combustion Institute* **36**, 3263-3270.

Ganser, GH (1993) A rational approach to drag prediction of spherical and nonspherical particles. *Powder Technology* **77**, 143-152.

Gould, JS, McCaw, W, Cheney, N, Ellis, P, Knight, I, Sullivan, A (2008) 'Project Vesta: fire in dry eucalypt forest: fuel structure, fuel dynamics and fire behaviour.' (Csiro Publishing:

Haider, A, Levenspiel, O (1989) Drag coefficient and terminal velocity of spherical and nonspherical particles. *Powder technology* **58**, 63-70.

Hölzer, A, Sommerfeld, M (2008) New simple correlation formula for the drag coefficient of non-spherical particles. *Powder Technology* **184**, 361-365.

Kortas, S, Mindykowski, P, Consalvi, JL, Mhiri, H, Porterie, B (2009) Experimental validation of a numerical model for the transport of firebrands. *Fire Safety Journal* **44**, 1095-1102.

Linteris, GT, Gewuerz, L, McGrattan, KB, Forney, GP (2004) Modeling solid sample burning with FDS. *National Institute of Standards and Technology, NISTIR* **7178**, 36.

Manzello, SL, Cleary, TG, Shields, JR, Yang, JC (2006) Ignition of mulch and grasses by firebrands in wildland–urban interface fires. *International Journal of Wildland Fire* **15**, 427-431.

Manzello, SL, Shields, JR, Cleary, TG, Maranghides, A, Mell, WE, Yang, JC, Hayashi, Y, Nii, D, Kurita, T (2008) On the development and characterization of a firebrand generator. *Fire Safety Journal* **43**, 258-268.

Manzello, SL, Suzuki, S (2013) Experimentally simulating wind driven firebrand showers in Wildland-Urban Interface (WUI) fires: overview of the NIST firebrand generator (NIST dragon) technology. *Procedia Engineering* **62**, 91-102.

Manzello, SL, Suzuki, S (2014) Exposing decking assemblies to continuous wind-driven firebrand showers. *Fire Safety Science* **11**, 1339-1352.

McArthur, AG (1967) Fire behaviour in eucalypt forests. Commonwealth of Australia, Department of National Development, , Canberra, Australia.

McGrattan, K, McDermott, R, Weinschenk, C, Overholt, K, Hostikka, S, Floyd, J (2015a) Fire dynamics simulator (Sixth Edition) user's guide. National Institute of Standards and Technology, Gaithersburg, Maryland, USA.

McGrattan, K, McDermott, R, Weinschenk, C, Overholt, K, Hostikka, S, Floyd, J (2015b) Fire Dynamics Simulator Technical Reference Guide Volume 1: Mathematical Model. National Institute of Standards and Technology, Gaithersburg, Maryland, USA.

Moinuddin, K, Razzaque, QS, Thomas, A (2020) Numerical simulation of coupled pyrolysis and combustion reactions with directly measured fire properties. *Polymers* **12**, 2075.

Perez-Ramirez, Y, Mell, WE, Santoni, P-A, Tramoni, J-B, Bosseur, F (2017) Examination of WFDS in Modeling Spreading Fires in a Furniture Calorimeter. *Fire Technology* **53**, 1795-1832.

Sardoy, N, Consalvi, J, Kaiss, A, Fernandez-Pello, A, Porterie, B (2008) Numerical study of ground-level distribution of firebrands generated by line fires. *Combustion and Flame* **154**, 478-488.

Stephen, DT, Fernandez-Pello, AC (1998) On the flight paths of metal particles and embers generated by power lines in high winds—a potential source of wildland fires. *Fire Safety Journal* **30**, 333-356.

Storey, MA, Price, OF, Bradstock, RA, Sharples, JJ (2020) Analysis of Variation in Distance, Number, and Distribution of Spotting in Southeast Australian Wildfires. *Fire* **3**, 10.

519 Suzuki, S, Johnsson, E, Maranghides, A, Manzello, SL (2016) Ignition of wood fencing assemblies
520 exposed to continuous wind-driven firebrand showers. *Fire Technology* **52**, 1051-1067.

521 Tarifa, CS (1967) Transport and combustion of firebrands. Instituto Nacional de Tecnica Aeroespacial,
522 Esteban Terradas No. FG-SP-114 and FG-SP-146, Madrid.

523 Tarifa, CS, del Notario, PP, Moreno, FG (1965) 'On the flight paths and lifetimes of burning particles
524 of wood, Symposium (International) on Combustion.' (Elsevier:

525 Thomas, C, Sharples, JJ, Evans, J (2020) The terminal-velocity assumption in simulations of long-range
526 ember transport. *Mathematics and Computers in Simulation* **175**, 96-107.

527 Thomas, JC, Mueller, EV, Santamaria, S, Gallagher, M, El Houssami, M, Filkov, A, Clark, K,
528 Skowronski, N, Hadden, RM, Mell, W, Simeoni, A (2017) Investigation of firebrand generation
529 from an experimental fire: Development of a reliable data collection methodology. *Fire Safety*
530 *Journal* **91**, 864-871.

531 Wadhwani, R (2019) Physics-based simulation of short-range spotting in wildfires. Victoria University.

532 Wadhwani, R, Sutherland, D, Moinuddin, K (2017a) Suitable pyrolysis model for physics-based
533 bushfire simulation. In '11th Asia-Pacific Conference on Combustion. University of Sydney,
534 Sydney', 10-14 December 2017. (Combustion Institute:

535 Wadhwani, R, Sutherland, D, Moinuddin, K (2019) 'Simulated transport of short-range embers in an
536 idealised bushfire, 6th International Fire Behavior and Fuels Conference.' Sydney, Australia,
537 April 29-May 3, 2019.

538 Wadhwani, R, Sutherland, D, Ooi, A, Moinuddin, K, Thorpe, G (2017b) Verification of a Lagrangian
539 particle model for short-range firebrand transport. *Fire Safety Journal* **91**, 776-783.

540 Wadhwani, R, Sutherland, D, Thorpe, G, Moinuddin, K, (2021) Improvement of drag model for non-
541 burning firebrand transport in Fire Dynamics Simulator *In Vervoort, R.W., Voinov, A.A., Evans,*
542 *J.P. and Marshall, L. (eds) MODSIM2021, 24th International Congress on Modelling and*
543 *Simulation. Modelling and Simulation Society of Australia and New Zealand, December 2021,*
544 *pp. 85–91. ISBN: 978-0-9872143-8-6.*

545

546

547 Table 1: Particle velocity components (u, v, w) measured for each case using two orthogonal
548 cameras.

Experimental cases	u (std. dev.) ($m.s^{-1}$)	v (std. dev.) ($m.s^{-1}$)	w (std. dev.) ($m.s^{-1}$)
Re1-non-burning	8.5 (1.49)	-0.3 (0.5)	0.8 (0.6)
Re2-non-burning	10 (1.65)	-0.5 (0.6)	0.7 (0.6)
Re2-burning	8.25 (1.15)	-0.3 (0.6)	0.2 (0.5)
Re2 -burning	9.55 (1.45)	-0.2 (0.6)	0.1 (0.6)

549

550

551 Table 2: List of drag models tested in this work

Sr. No.	Drag model	Drag correlation
1	FDS Spherical drag model (McGrattan *et al.* 2015b)	$C_{D,sph} = \begin{cases} \frac{24}{Re_D} & , \ Re_D < 1 \\ \frac{24(0.85+0.15Re_D^{0.687})}{Re_D}, & 1 < Re_D < 1000 \\ 1 & , \ Re_D > 1000 \end{cases}$ (3)
2	Haider & Levenspiel drag model (Haider and Levenspiel 1989)	$C_{D,Ha} = \frac{24}{Re_D}\left(1 + ARe_D^B\right) + \frac{C}{1+\frac{D}{Re_D}}$, $Re_D < 2.6 \times 10^5$ (4) where $A = \exp(2.3288 - 6.4581\psi + 2.4486\psi^2)$ $B = 0.0964 + 0.5565\psi$ $C = \exp(4.905 - 13.8944\psi + 18.4222\psi^2 - 10.2599\psi^3)$ $D = \exp(1.4681 + 12.2584\psi - 20.7322\psi^2 + 15.8855\psi^3)$ Ψ= Sphericity of the particle
3	Ganser drag model	$\frac{C_{D,Ga}}{K_2} = \frac{24}{Re_D K_1 K_2}(1 + 0.1118(Re_D K_1 K_2)^{0.6567}) + \frac{0.4305}{1+\frac{3305}{Re_D K_1 K_2}}$, $Re_D K_1 K_2 \leq 10^5$ (5)

	(Ganser 1993)	where K_1 & K_2 is Shape factor in Stokes and Newton regimes For isometric particle, $K_1 = [0.3333 + 0.6667\psi^{-0.5}]^{-1}$ and $K_2 = 10^{1.8148(-\log\psi)^{0.5743}}$
4	Hölzer & Sommerfeld drag model (Hölzer and Sommerfeld 2008)	$C_{D,Ho} = \frac{8}{Re_D\sqrt{\psi_\perp}} + \frac{16}{Re_D\sqrt{\psi}} + \frac{3}{\sqrt{Re_D}\ \psi^{0.75}} + 0.42\ 10^{0.4(-\log\psi)^{0.2}} \frac{1}{\psi_\perp}$, $Re_D \leq 10^7$ (6) where $\psi_\perp$ is called as a crosswise sphericity
5	Bagheri & Bonadonna drag model (Bagheri and Bonadonna 2016)	$C_{D,Ba} = \frac{24k_S}{Re_D}\left(1 + 0.125\left(Re_D\frac{k_N}{k_S}\right)^{2/3}\right) + \frac{0.46k_S}{1+\frac{5330}{Re_D\frac{k_N}{k_S}}}, Re_D < 3\times10^5$ (7) where $k_S = \frac{\left(F_S^{1/3}+F_S^{-1/3}\right)}{2}$, $k_N = 10^{\alpha_2[-\log(F_N)]\beta_2}$, $\alpha_2 = 0.45 + \frac{10}{\exp(2.5\log(\rho')+30)}$, $\beta_2 = 1 - \frac{37}{\exp(3\log(\rho')+100)}$ $\text{apparent density}(\rho') = \frac{\rho_{solid,\ particle}}{\rho_{fluid,\ air}}$, $F_S = fe^{1.3}\frac{d_{eq}^3}{LIS}$

		$F_N = f^2 e \frac{d_{eq}^3}{L I S}$, flatness of particle$(f) = S/I$, elongation of particle$(e) = I/L$, and d_{eq}=equivalent diameter of particle

552

553

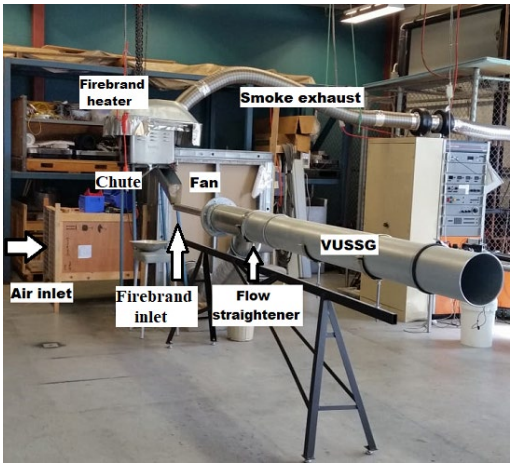

(a) front-view of firebrand generator

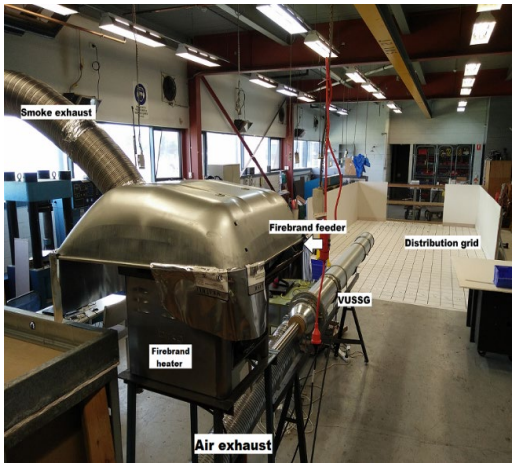

(b) back-view of firebrand generator

(c) firebrand heater producing firebrand

s

(d) flow straightener section

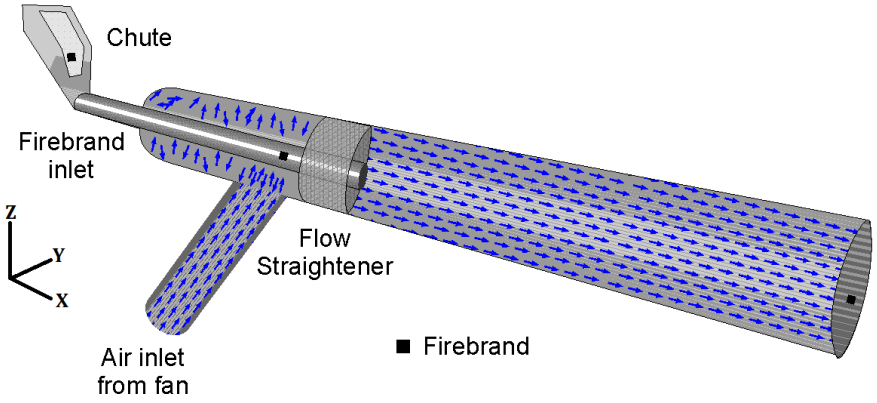

(e) a cutaway schematic of firebrand generator

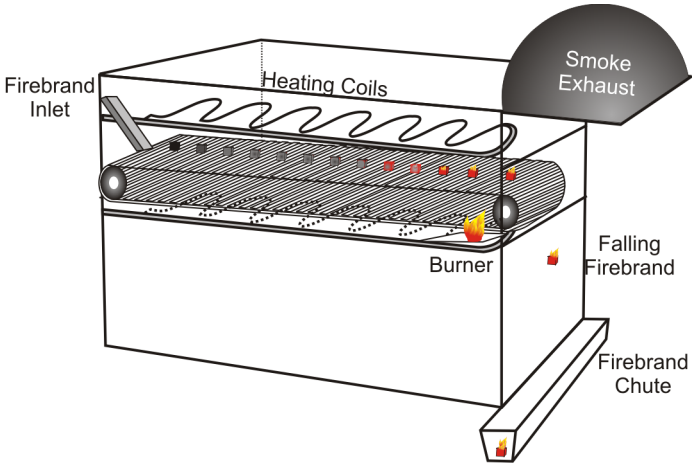

(f) schematic of the firebrand heater and ignition arrangement

Fig. 1: Different sections of firebrand generator highlighting its working principles and hidden features

554

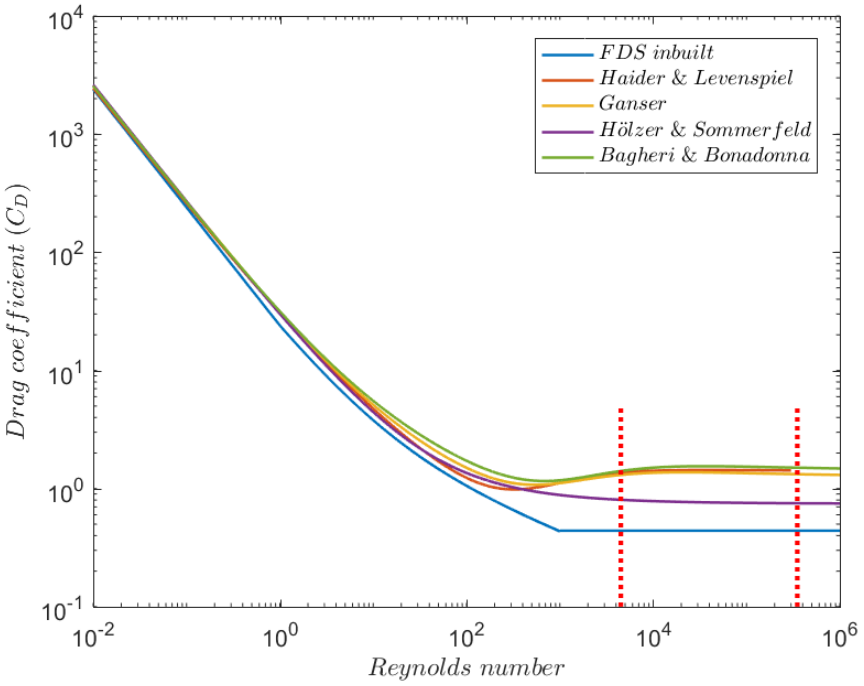

Fig. 2: Variation of different drag models (listed in Table 2) in estimating drag coefficient with Reynolds numbers (corresponding to V_{centre} 23.4 and 25.9 m.s^{-1}) considered in present study for cubiform firebrand. Two dotted red lines shows the variation of Reynolds number during the flight time of firebrand

555

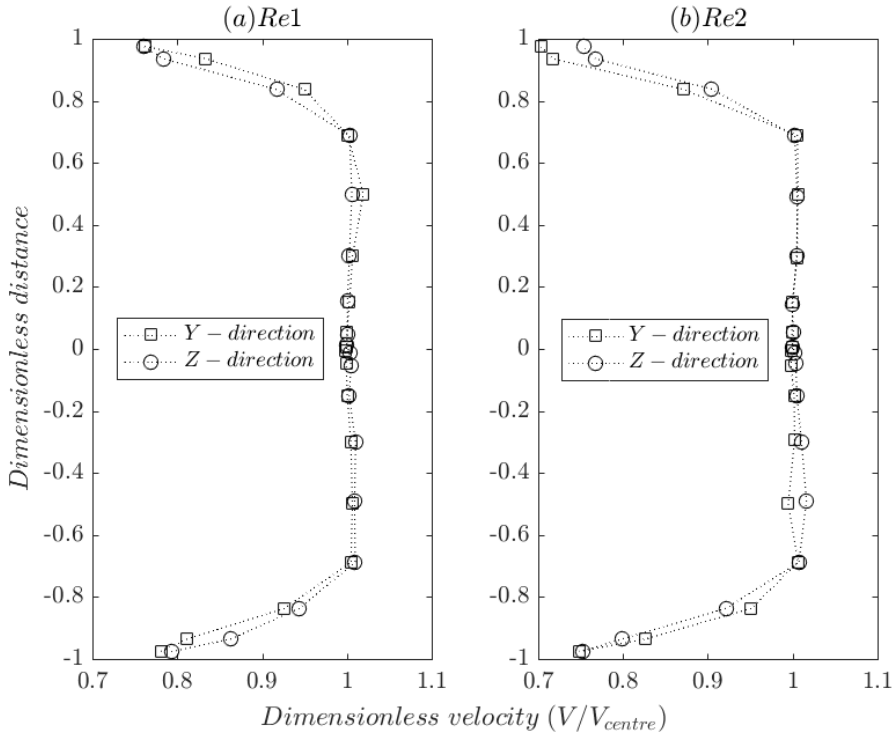

Fig. 3: Flow profile measured at the mouth of the generator using pitot tube

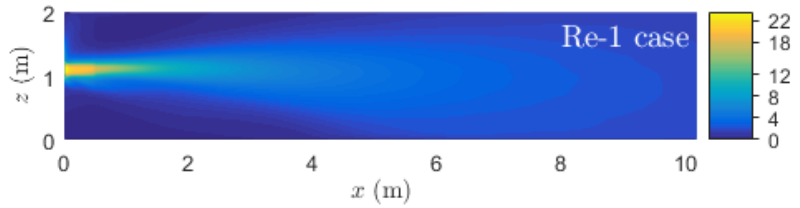

(a) Re1-flow

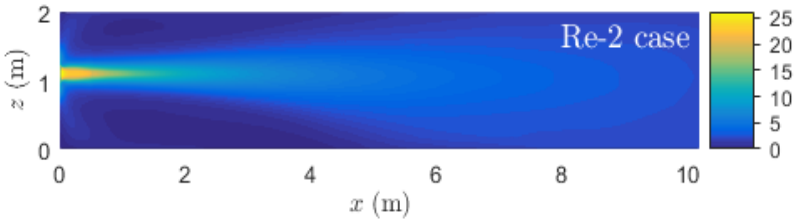

(b) Re2-flow

Fig.4: Simulated mean speed contours of the generator for two flow speeds. Note that the jet for the Re1 flow is more defuse than for the Re2 flow. For the Re1 flow the jet starts to decay significantly around 2.5 m, whereas for the Re2 flow the jet starts to decay significantly around 3.5 m.

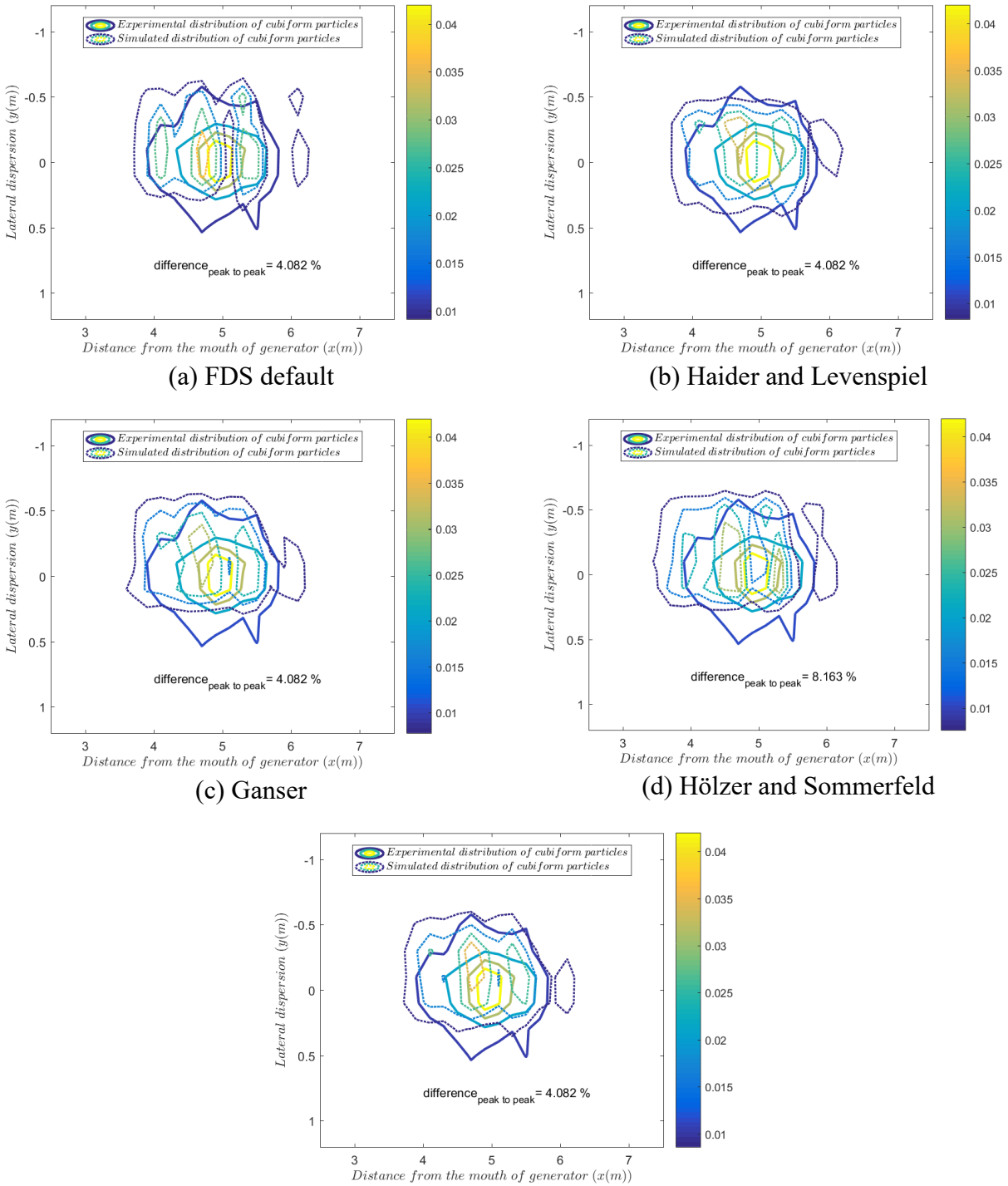

(a) FDS default

(b) Haider and Levenspiel

(c) Ganser

(d) Hölzer and Sommerfeld

(e) Bagheri and Bonadonna

Fig. 5: Comparative contours (experimental and simulated) of firebrand distribution for non-burning cubiform particles at Re1 with all the drag models

559

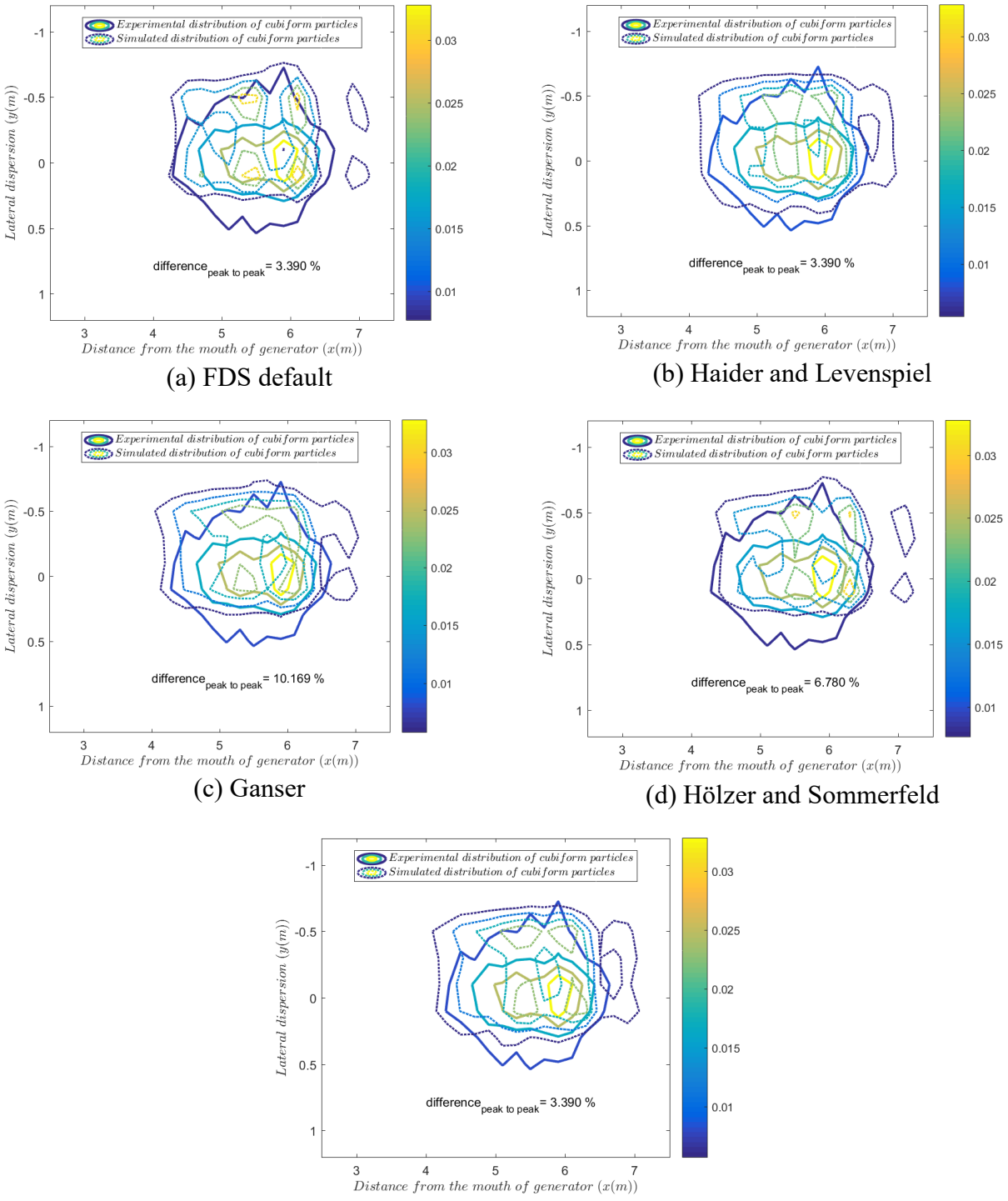

(a) FDS default

(b) Haider and Levenspiel

(c) Ganser

(d) Hölzer and Sommerfeld

(e) Bagheri and Bonadonna

Fig. 6: Comparative contours (experimental and simulated) of firebrand distribution for non-burning cubiform particles at Re2 with all the drag models

560

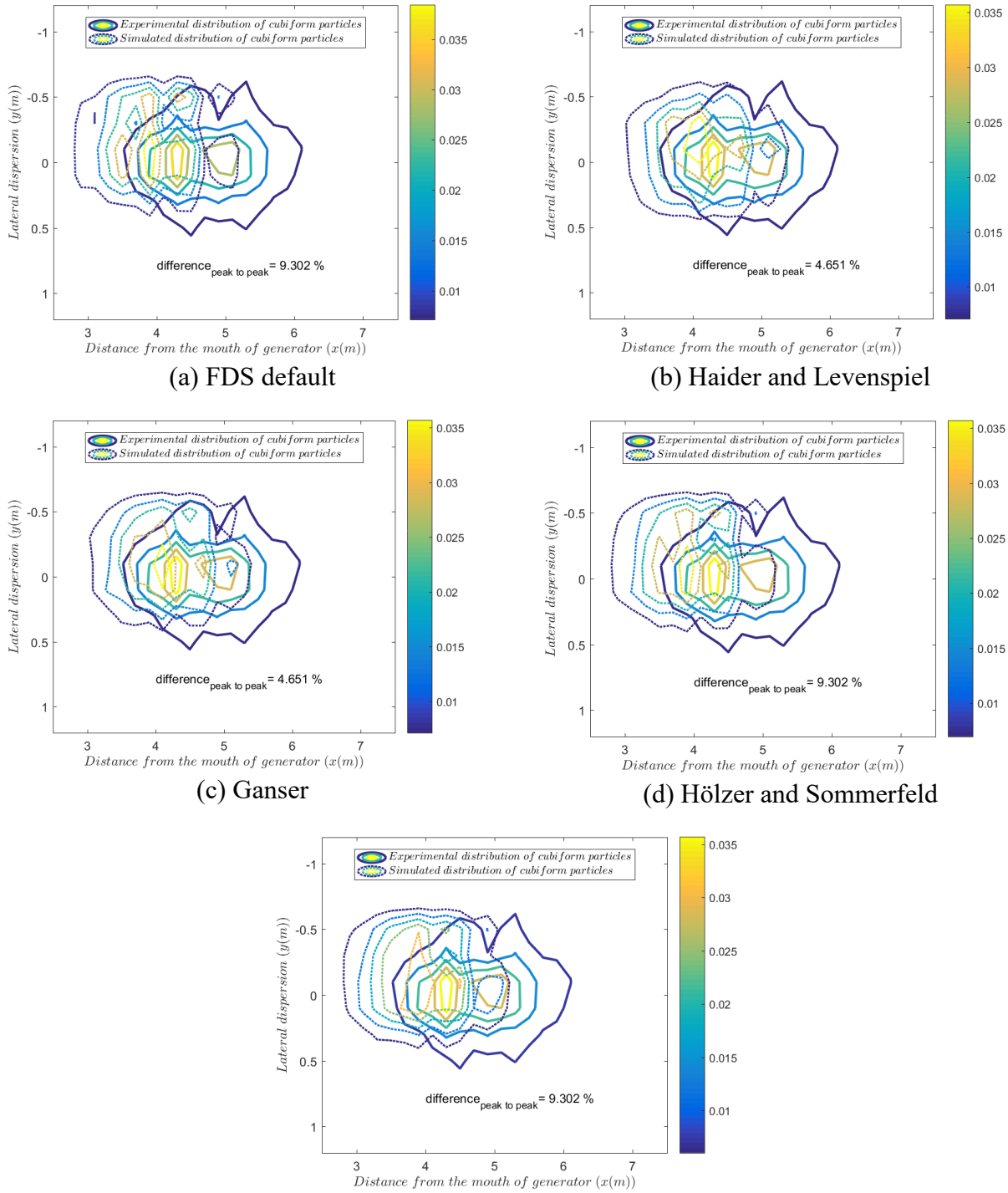

(a) FDS default

(b) Haider and Levenspiel

(c) Ganser

(d) Hölzer and Sommerfeld

(e) Bagheri and Bonadonna

Fig. 7: Comparative contours (experimental and simulated) of firebrand distribution for burning cubiform particles at Re1 with all the drag models

561

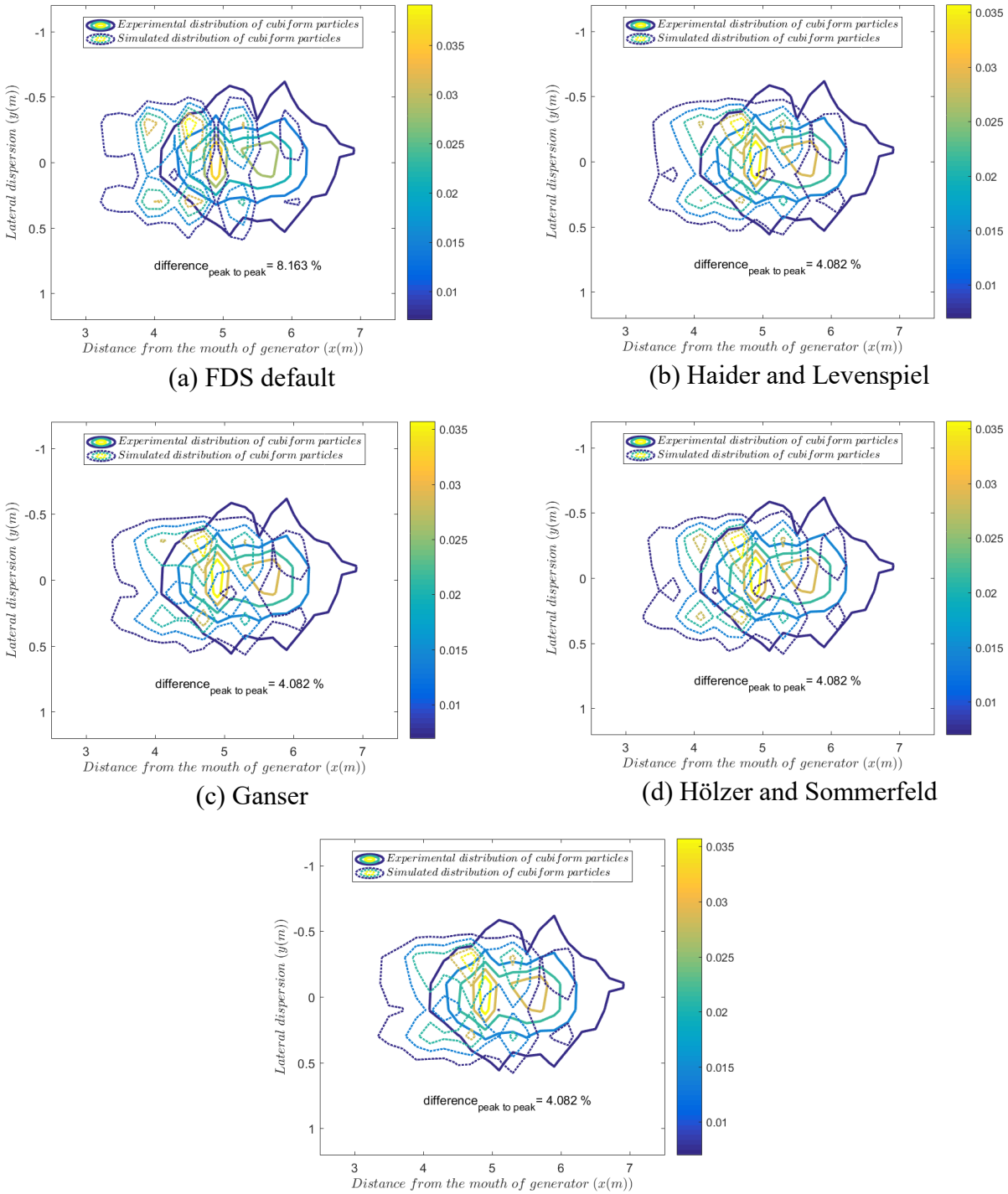

Fig. 8: Comparative contours (experimental and simulated) of firebrand distribution for burning cubiform particles at Re2 with all the drag models

562

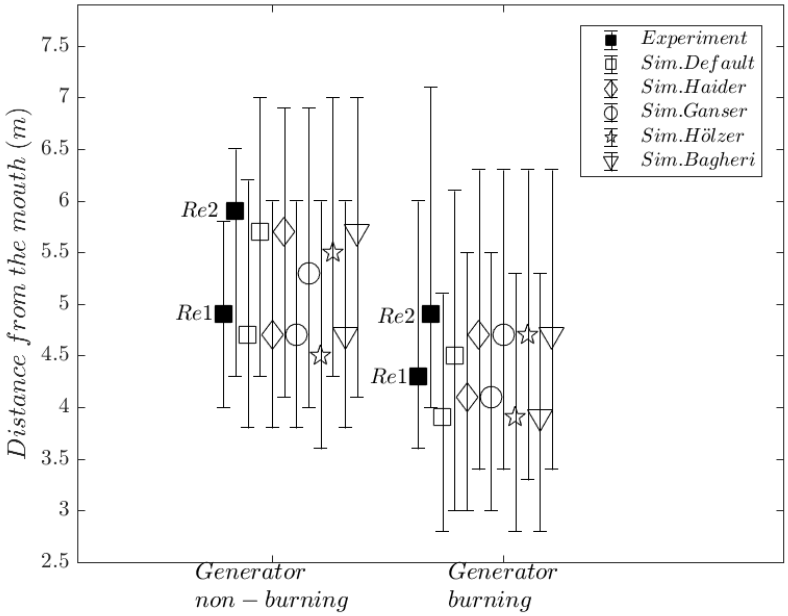

563

564 **Fig. 9**: Comparison between the observed experimental and simulated peaks of firebrand
565 distribution using full-scale generator with different drag models. The whiskers represent the
566 maximum and minimum distances of particle transport.